IEEE Access
Multidisciplinary | Rapid Review | Open Access Journal

Received August 1, 2018, accepted September 21, 2018, date of publication October 2, 2018, date of current version October 29, 2018.

Digital Object Identifier 10.1109/ACCESS.2018.2873484

Multi-Contrast Brain MRI Image Super-Resolution With Gradient-Guided Edge Enhancement

HONG ZHENG[1,2], KUN ZENG[1], DI GUO[3], JIAXI YING[1], YU YANG[1], XI PENG[4], FENG HUANG[5], ZHONG CHEN[1], AND XIAOBO QU[1]

[1]Fujian Provincial Key Laboratory of Plasma and Magnetic Resonance, Department of Electronic Science, College of Physical Science and Technology, Xiamen University, Xiamen 361005, China
[2]Key Laboratory of Intelligent Processing of Image and Graphics, School of Computer Science and Information Security, Guilin University of Electronic Technology, Guilin 541004, China
[3]School of Computer and Information Engineering, Fujian Provincial University Key Laboratory of Internet of Things Application Technology, Xiamen University of Technology, Xiamen 361024, China
[4]Shenzhen Institutes of Advanced Technology, Chinese Academy of Sciences, Shenzhen 518055, China
[5]Neusoft Medical System, Shanghai 110179, China

Corresponding author: Xiaobo Qu (quxiaobo@xmu.edu.cn)

This work was supported in part by the National Key R&D Program of China under Grant 2017YFC0108703, in part by the National Natural Science Foundation of China under Grant 61571380, Grant 61871341, Grant 61811530021, Grant U1632274, Grant 61672335, and Grant 61601389, in part by the Natural Science Foundation of Fujian Province of China under Grant 2018J06018 and Grant 2016J05205, in part by the Fundamental Research Funds for the Central Universities under Grant 20720180056, and in part by the Science and Technology Program of Xiamen under Grant 3502Z20183053.

ABSTRACT In magnetic resonance imaging (MRI), the super-resolution technology has played a great role in improving image quality. The aim of this paper is to improve edges of brain MRI by incorporating the gradient information of another contrast high-resolution image. Multi-contrast images are assumed to possess the same gradient direction in a local pattern. We proposed to establish a relation model of gradient value between different contrast images to restore a high-resolution image from its input low-resolution version. The similarity of image patches is employed to estimate intensity parameters, leading a more accurate reconstructed image. Then, an iterative back-projection filter is applied to the reconstructed image to further increase the image quality. The new approach is verified on synthetic and real brain MRI images and achieves higher visual quality and higher objective quality criteria than the compared state-of-the-art super-resolution approaches. The gradient information of the multi-contrast MRI images is very useful. With a proper relation model, the proposed method enhances image edges in MRI image super-resolution. Improving the MRI image resolution from very low-resolution observations is challenging. We tackle this problem by first modeling the relation of gradient value in multi-contrast MRI and then performing fast supper-resolution methods. This relation model may be helpful for other MRI reconstruction problems.

INDEX TERMS MRI, image reconstruction, super-resolution, multi-contrast images.

I. INTRODUCTION

In magnetic resonance imaging (MRI), the low-resolution (LR) is usually encountered due to acquisition constrains such as limited sampling time or moving subjects. These LR may seriously affect the post-processing and medical diagnosis. To recover a high-resolution (HR) image from its low-resolution version [1], super-resolution technologies have been widely used in MRI [2]–[11].

Super-resolution methods can be roughly grouped into two main categories: Interpolation and non-interpolation. Interpolation approaches, e.g., the bicubic and bi-spline, are usually fast but frequently generate over-smooth images. Non-interpolation methods incorporate various image priors, e.g., sparse representation [3]–[6], [11] non-local reconstruction [7], [10] and total variations [8], [9], leading to more attractive super-resolved images. However, these non-interpolation methods usually require time-consuming iteration processing and do not pay special attention to edge information.

Edge structures of medical images have a particularly significant impact on visual scenes to detect suspicions, classify malformations and make diagnosis [15]. Thus, it is valuable to consider edge factor in image super-resolution. For example, edges are preserved pretty well in a contrast-guided interpolation (CGI) approach [16]. Edges are also sharpened by considering gradient features [2], [12]. These methods,

only explore the information from a single target image in the low resolution, thus a faithful super-resolution may be hard to achieve since the available information is very limited.

Other prior information beyond a single image is expected to improve the image resolution [5], [7], [13], [14], [17], [18]. For example, non-local similarity of image patches is introduced as the prior information [5], [7], [13], [14], [17]. These methods also require time-consuming iteration processing. In addition, Zheng *et al.* [18] introduced a fast interpolation approach using the local weight similarity (ILWS) between multi-contrast brain images to improve the resolution of the LR MRI image. But, it does not perform satisfactorily when the LR image is too smooth.

Recently, an effective interpolation method that establishing gradient relations between the LR image and HR reference image with different contrast was proposed [19] in the remote sensing. This method has a simple but effective non-iterative linear model, and does not require training sets. Image edges were interpolated much well according to the reported results [19]. This model is called as the Super-Resolution of using Gradient Relations (SRGR) model here. The SRGR provides a promising direction to model relationship between the multi-contrast images due to its fast computing and attractive performance. The SRGR, as far as we know, has not been applied for MRI. What is more, to fit for the multi-contrast MRI interpolation, SRGR should be carefully modified since the images in MRI are very different from those in remote sensing [19]. This aim of this work is to model the gradient relations of multi-contrast MRI images and improve MRI super-resolution.

In this work, we propose a new gradient linear relation model for multi-contrast brain MRI super-resolution, which is inspired by SRGR. The gradient information on edges of a HR reference is used to guide the interpolation of a LR MRI image. To further improve the resolution, the non-local similarity of image patches is employed to robustly estimate the intensity parameter of the model and the Iterative Back-Projection (IBP) filter is enforced. Experimental results will verify more promising results for our method than the compared MRI interpolation approaches.

This paper is structured as follows. Section II gives a brief review of the related work. Section III presents the proposed approach. Section IV provides experimental results followed by discussions in Section V. Finally, we summarize this work in Section VI.

II. BACKGROUND AND RELATED WORKS

A. MULTI-CONTRAST IMAGES IN MRI

Multi-contrast images are frequently acquired in MRI [1], [20] and the commonly acquired ones are T1w and T2w. Plentiful edge structures are visible in these two contrast images of the same subject (Fig. 1). According to the MRI physics [21], the image $S(\vec{r})$ of T1w or T2w is generated as follows:

$$S(\vec{r}) \propto \rho(\vec{r})\left(1 - e^{-TR/T_1(\vec{r})}\right)\left(e^{-TE/T_2(\vec{r})}\right), \quad (1)$$

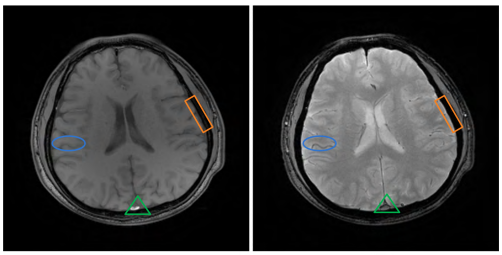

(a) (b)

FIGURE 1. Multi-contrast MRI brain images: (a) a T1w image; (b) a T2w image.

where $\rho(\vec{r})$ is the proton density at spatial location $\vec{r}$, TR refers to the repetition time and TE denotes the echo time. By setting different values of TR and TE, multi-contrast images will be acquired. Yet, these images share the proton density of the subject and hence they largely share similar anatomical structures but with different contrasts in regions. The shared information between inter-contrast images was previously considered to profit the super-resolution [18] and other image reconstruction tasks [22]–[24].

B. BRIEF REVIEWS OF SRGR MODEL

The SRGR model was proposed in super-resolution of remote sensing images [19]. Its basic idea is described below.

Suppose that a LR image $\tilde{\mathbf{X}}_L$ of its target HR image $\tilde{\mathbf{X}}$ (Fig. 2(a)) and a HR reference image $\tilde{\mathbf{R}}$ (Fig. 2(b)) are available while $\tilde{\mathbf{X}}$ and $\tilde{\mathbf{R}}$ have same size. SRGR consists two steps: 1) A pre-interpolated image $\mathbf{X}$ (Fig. 2(c)), that is with the same size of $\tilde{\mathbf{X}}$, is obtained with some classic interpolation methods; 2) Gradient information from $\tilde{\mathbf{R}}$ is applied to update $\mathbf{X}$.

To improve the interpolation, the same gradient direction is assumed between the multi-contrast images $\tilde{\mathbf{X}}$ and $\tilde{\mathbf{R}}$. The relationship of gradient is modeled as [19]

$$\frac{g(\tilde{X}_{i,j})}{g(\tilde{R}_{i,j})} = \lambda^0, \quad (2)$$

where $g(\cdot)$ is a second order gradient function, $\tilde{X}_{i,j}$ is the pixel of $\tilde{\mathbf{X}}$, $\tilde{R}_{i,j}$ is the pixel of $\tilde{\mathbf{R}}$ and λ^0 is a parameter that models this relationship ideally.

Assuming that an adjustment parameter $\delta_{i,j}$ is added to the (i,j) pixel $X_{i,j}$ of a pre-interpolated image $\mathbf{X}$, the SRGR model is formulated as [19]

$$\min_{\delta_{i,j}}\{[g(X_{i,j}+\delta_{i,j}) - \lambda g(\tilde{R}_{i,j})]^2 + [g_\perp(X_{i,j}+\delta_{i,j}) - \lambda_\perp g_\perp(\tilde{R}_{i,j})]^2\} \quad (3)$$

by considering a gradient direction l (Fig. 2(d)) and its normal direction, also called edge direction, $l_\perp$ (Fig. 2(d)).

Now, we are prepared to discuss the essential parts in Eq. (3). First, the gradient functions $g(X_{i,j}+\delta_{i,j})$ and $g_\perp(X_{i,j}+\delta_{i,j})$ are defined as

$$\begin{aligned} g(X_{i,j}+\delta_{i,j}) &= X_{i+1,j-1} + X_{i-1,j+1} - 2(X_{i,j}+\delta_{i,j}) \\ g_\perp(X_{i,j}+\delta_{i,j}) &= X_{i-1,j-1} + X_{i+1,j+1} - 2(X_{i,j}+\delta_{i,j}) \end{aligned} \quad (4)$$

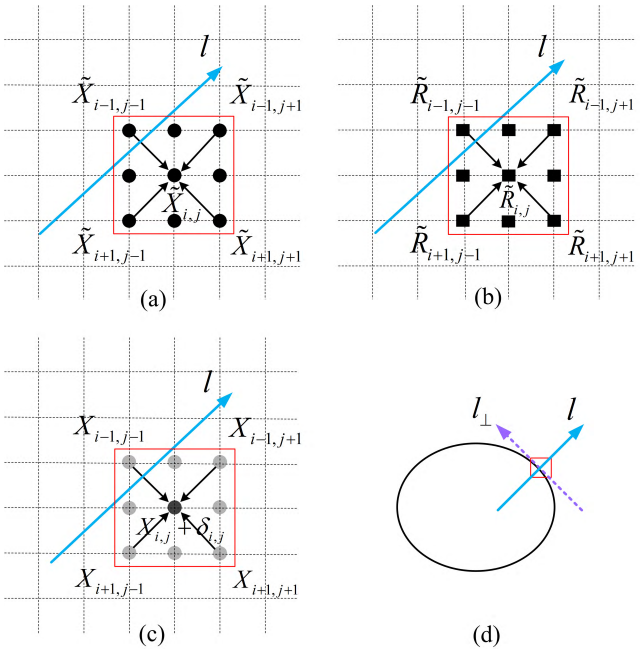

FIGURE 2. Illustration for SRGR model in a local pattern. (a) is the target HR image $\tilde{\mathbf{X}}$; (b) is the HR reference image $\tilde{\mathbf{R}}$ with different contrast; (c) is the pre-interpolated image $\mathbf{X}$ obtained from the low observation of $\tilde{\mathbf{X}}$; (d) An example of the gradient direction $\boldsymbol{l}$ in a local pattern and the edge direction. Note: The gradient direction is denoted by the vector $\boldsymbol{l}$. In estimation, a more accurate pixel, e.g. $\boldsymbol{X_{i,j}+\delta_{i,j}}$, indicated by dark circles within (c) is used to replace the pre-interpolated HR pixel, e.g. $\boldsymbol{X_{i,j}}$, to generate a better HR image.

where $X_{i+1,j-1}$ and $X_{i-1,j+1}$ are the neighborhood pixels of $X_{i,j}$ along the direction l, while $X_{i-1,j-1}$ and $X_{i+1,j+1}$ are the nearest neighbors of $X_{i,j}$ along the direction $l_\perp$, respectively. Second, the λ and $\lambda_\perp$ in Eq. (3) are parameters that adjusting intensity in two directions. Too smaller λ and $\lambda_\perp$ will lead to blur edges. On the contrary, too larger λ and $\lambda^\perp$ will cause artificial edges [19]. In SRGR, their values are estimated as

$$\begin{aligned}\lambda &= (X_{i+1,j-1} - X_{i-1,j+1})/(\tilde{R}_{i+1,j-1} - \tilde{R}_{i-1,j+1})\\ \lambda_\perp &= (X_{i-1,j-1} - X_{i+1,j+1})/(\tilde{R}_{i-1,j-1} - \tilde{R}_{i+1,j+1}).\end{aligned} \quad (5)$$

Overall, the SRGR model in Eq. (3) tries to refine the pixels of pre-interpolated image by minimizing the consistent second order gradient that is parallel and perpendicular to the edges. Since each term in this model is quadratic, Eq. (3) can be solved fast by forcing the first derivative of the objective function to be zero. More details of implementation can be found in [19].

However, the basic SRGR may not suit well for recovering MRI since the local-contrast may be more complex than the remote sensing images presented in [19]. How to modify the SRGR to fit for multi-contrast MRI will be the main focus of our work.

III. PROPOSED METHOD

An overview of the proposed approach is summarized in Fig. 3. First, the LR image is pre-interpolated by the CGI method. Second, the HR reference image is registered to pre-interpolated image (Benefit of registration is shown in Appendix C). Then, the HR image of interest will be restored by using the gradient information of the registered HR reference image in another contrast. Finally, the HR image will be enhanced with an IBP filter. In the following, the essential parts of the proposed method will be presented.

A. MEASURING GRADIENT DIFFERENCE ON SAME CONTRAST IMAGES

The essence of SRGR model in Eq. (3) is to estimate the relationship of the second gradient order between the pre-interpolated image $\mathbf{X}$ and the HR reference image $\tilde{\mathbf{R}}$. Now, let us consider an ideal step. Assume that an ideal pre-interpolation can generate a HR image $\mathbf{X}$ that is as good as the target HR image $\tilde{\mathbf{X}}$. Accordingly, there may exist a pre-interpolated reference image $\mathbf{R}$ that is as good as $\tilde{\mathbf{R}}$. Then, according to Eq. (2), the following relationship holds true

$$\frac{g(X_{i,j})}{g(R_{i,j})} \approx \lambda^0, \quad (6)$$

where $R_{i,j}$ is the (i, j) pixel of $\mathbf{R}$. Through the elementary mathematical manipulation of Eqs. (2) and (6), one obtains

$$\lambda^{0'} = \frac{g(\tilde{X}_{i,j}) - g(X_{i,j})}{g(\tilde{R}_{i,j}) - g(R_{i,j})} \approx \lambda^0, \quad (7)$$

which is the ratio of gradient difference estimated from the same contrast images.

The Eq. (7) implies that one may turn to measure the ratio of the gradient difference for the pairs of target/pre-interpolated images and reference/pre-interpolated reference images. This modification is important since the gradient difference is computed within one contrast, but not across two contrasts in the original SRGR in Eq. (2). Thus, Eq. (7) is able to reduce the effect of large contrast variations on degrading the multi-contrast MRI super-resolution, which will be systematically analyzed in the following section.

B. SUPER-RESOLUTION MODEL

Based on Eq. (7), our model can be expressed as

$$\begin{aligned}\min_{\delta_{i,j}}\{&[(g(X_{i,j}+\delta_{i,j}) - g(X_{i,j})) - \lambda(g(\tilde{R}_{i,j}) - g(R_{i,j}))]^2\\ &+ [(g_\perp(X_{i,j}+\delta_{i,j}) - g_\perp(X_{i,j}))\\ &- \lambda_\perp(g_\perp(\tilde{R}_{i,j}) - g_\perp(R_{i,j}))]^2\}\end{aligned} \quad (8)$$

which finds refinements on pixels to minimize the gradient difference between the HR images and HR reference images.

In this model, the accuracy of λ and $\lambda_\perp$ is essential for image reconstruction. Thus, error analysis on λ (same analysis for $\lambda_\perp$ is omitted) and edge pixels will be briefly given below (More details can be found in Appendix A). The following analysis will show that, comparing with the SRGR, the new method will obtain lower reconstruction error on edge pixels.

In our model, the error on λ is denoted by $\Delta\lambda'$ defined as

$$\Delta\lambda' = \lambda^{0'} - \lambda, \quad (9)$$

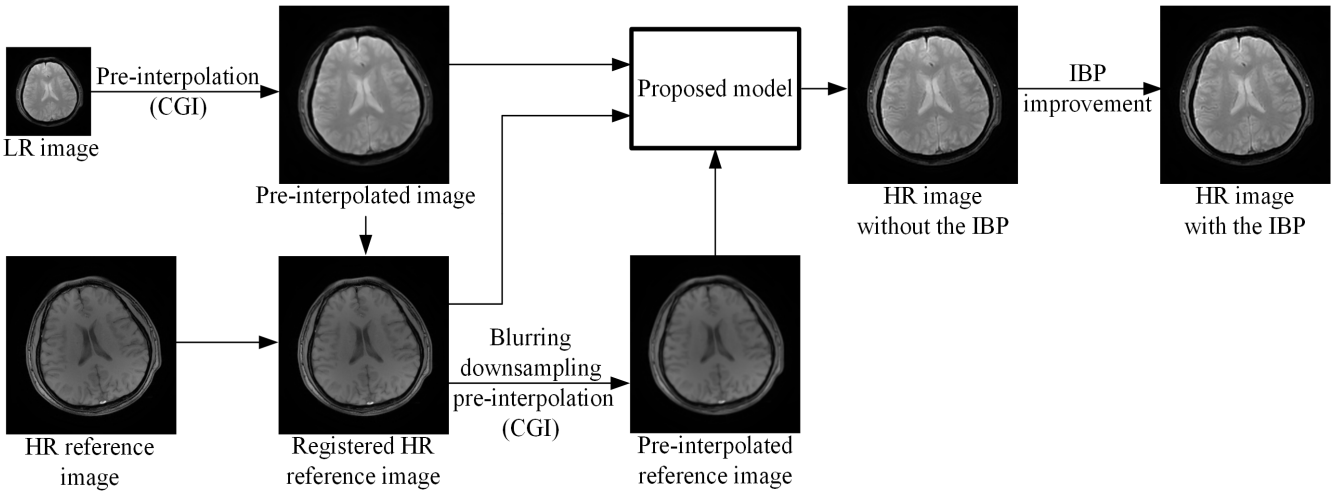

FIGURE 3. Block diagram of the proposed method.

and the reconstruction error on edge pixels is denoted by $\Delta\delta'_{i,j}$. According to Eq. (8), we know that

$$\Delta\delta'_{i,j} \propto \Delta\lambda'[g(\tilde{R}_{i,j}) - g(R_{i,j})]. \tag{10}$$

In SRGR model (Eq. (3)), the error $\Delta\lambda$ is

$$\Delta\lambda = \lambda^0 - \lambda. \tag{11}$$

and its reconstruction error $\Delta\delta_{i,j}$ is determined as

$$\Delta\delta_{i,j} \propto \Delta\lambda g(\tilde{R}_{i,j}). \tag{12}$$

Then, since $\lambda^{0'} \approx \lambda^0$ in Eq. (7), combing Eqs. (9) and (11) we will get

$$\Delta\lambda \approx \Delta\lambda'. \tag{13}$$

In addition, most edge pixels in the HR reference image $\tilde{R}_{i,j}$ and the pre-interpolated reference image $R_{i,j}$ satisfy (More details are provided in Appendix A)

$$\left|g(\tilde{R}_{i,j}) - g(R_{i,j})\right| < \left|g(\tilde{R}_{i,j})\right|. \tag{14}$$

Finally, by comparing Eq. (10) with Eq. (12), it can be concluded that the condition

$$\left|\Delta\delta'_{i,j}\right| < \left|\Delta\delta_{i,j}\right| \tag{15}$$

holds for most edge pixels. This indicates, in our model, the reconstruction error of edge pixels is mostly smaller than that of SRGR.

Above analysis can be verified in MRI images with smooth pixels at the boundary of two contrast regions, such as the laminar structure [7] in brain. The brain MRI image possesses the characteristics of laminar structure which is formed by the brain gyri and sulci [7]. In Figs. 4(a) and 4(b), one pair of multi-contrast toy examples which imitate local laminar structures is presented. With arbitrarily changing local contrasts, both Eqs. (14) and (15) are often satisfied as shown in Figs. 4(c) and 4(d), respectively. Analysis on more complex

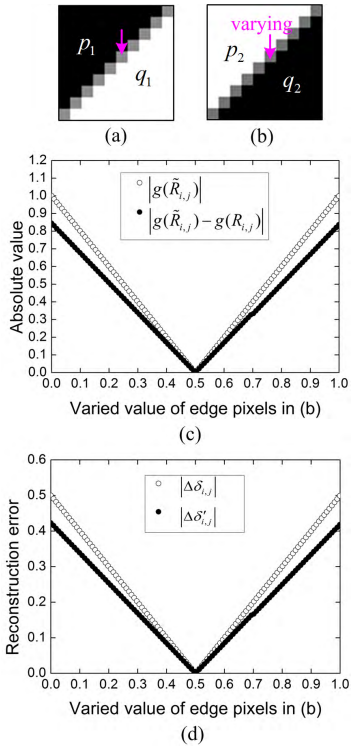

FIGURE 4. Error analysis on a toy example with the characteristics of laminar structure. (a) is the HR original image, in which $p_1 = 0$, $q_1 = 1$ and the edge pixel value is the average of p_1 and q_1; (b) is the HR reference image, in which $p_2 = 1$, $q_2 = 0$ and the edge pixel value changes from 0 to 1. This change of edge pixel value is embodied on the horizontal axis of Fig. 3(c-d). (c) Curves for $\left|g(\tilde{R}_{i,j})\right|$ and $\left|g(\tilde{R}_{i,j}) - g(R_{i,j})\right|$ of the edge pixel. (d) Curves for reconstruction errors.

images, e.g. Brainweb MRI [25], is given in Fig. 5. The average reconstruction error is measured as the root mean square error between the reconstructed pixel value and the original pixel value. Fig. 5(e) implies that Eq. (15) also holds true (More details of Figs.4 and 5 are presented in Appendix B).

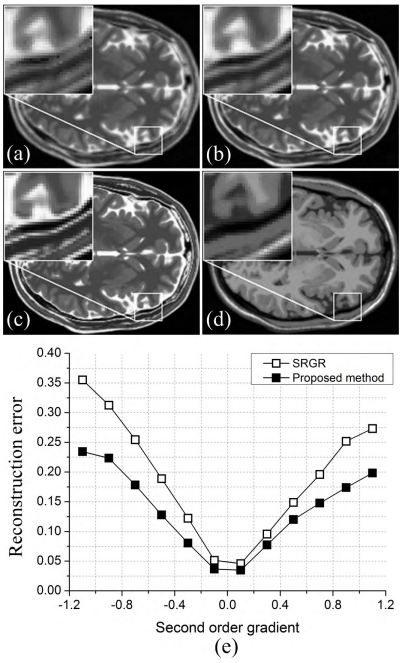

FIGURE 5. Comparison of reconstruction errors on Brainweb MRI data. (a) HR image using SRGR model, the PSNR = 21.54; (b) HR image using the proposed model, the PSNR = 24.17; (c) original T2w image (ground truth); (d) original T1w image (HR reference). (e) Mean error of reconstructed HR pixel values versus second order gradients.

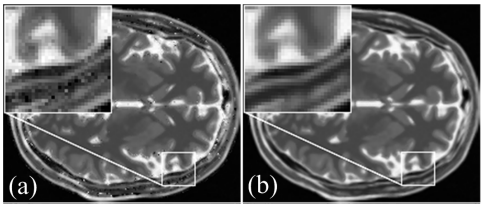

FIGURE 6. Reconstruction comparisons of λ and λ_Ω on Brainweb MRI data. (a) HR image produced with using λ; (b) HR image using the proposed model (i.e., λ_Ω are exploited), the PSNR = 23.85. Note: the ground truth and HR reference images are presented in Fig. 5(c) and (d), respectively.

C. ROBUST ESTIMATION FOR λ AND $\lambda_\perp$

We further propose a robust estimation for λ (the same method for $\lambda_\perp$). We assume that λ is the same for all similar patches within a local region Ω. First, we search similar patches in Ω using a fast global search method that exploring the same geometric direction for patches is adopted [22], [26], [27]. Then, the λ is computed for each patch according to Eq. (5). Last, the λ for all similar patches are averaged to a final λ_Ω for these patches. Improvement on estimating λ with similar patches is shown in Fig. 6, indicating that λ_Ω successfully avoids abnormal-pixel-values encountered using different λ for different patches.

D. IMAGE IMPROVEMENT WITH IBP

As we discussed before, the CGI method is utilized to perform the initial interpolation on the original LR image to produce the pre-interpolated image. Edge pixels in the pre-interpolated image are reconstructed one by one (in the order: from top left to bottom right) by our model and replace original residents of the pre-interpolated image. Finally, the HR image with more sharp and distinct edges will be obtained.

In order to take into account MRI acquisition properties, we impose Iterative Back-Projection (IBP) on the reconstructed HR pixels. The IBP iteratively minimizes the differences between the original LR image and LR version of the reconstructed HR image. Previously, in MRI super-resolution field, IBP was used for recovering image details in LR brain images [6], [28].

The IBP process is given by

$$(\mathbf{X}+\boldsymbol{\delta})^{(t+1)} = (\mathbf{X}+\boldsymbol{\delta})^{(t)} + (\mathbf{U}(\tilde{\mathbf{X}}_L - \mathbf{DS}(\mathbf{X}+\boldsymbol{\delta})^{(t)}))\mathbf{P} \quad (16)$$

where $(\mathbf{X}+\boldsymbol{\delta})^{(t)}$ denotes the estimated HR image after the t^{th} iterative calculation, and $\tilde{\mathbf{X}}_L$ denotes the original LR image. $\mathbf{P}$ is the back project filter, $\mathbf{S}$ is the blurring filter, $\mathbf{D}$ is the down-sampling operator and $\mathbf{U}$ is the up-sampling operator whose factor is the same with $\mathbf{D}$. More details and analysis about IBP can be found in [29].

For MRI images, IBP will improve the PSNR (Fig. 7(a)) of reconstruction by increasing the number of iterations (denoted by k) in the IBP. Considering the computation complexity, we choose $k = 5$ for all experiments in this paper, which generally yields satisfactory results (Fig. 7(d)).

IV. RESULTS

In this section, the proposed approach will be compared with the bicubic interpolation, the state-of-the-art CGI [16] and the ILWS that considers the multi-contrast images [18]. Experiments are conducted on Brainweb brain images and real MRI images. All methods run on a personal computer with Dual-Core CPU 3.00GHz and 2 GB memory.

Two objective criteria, the peak signal-to-noise ratio (PSNR) and the structural similarity (SSIM) [30], are exploited to quantitatively evaluate the super-resolution results. The higher PSNR indicates that the reconstructed image is more consistent to the original HR image and the higher SSIM implies that more accurate image structures are preserved.

A. SIMULATION SET UP

Before conducting reconstructions, a LR image is generated from an original HR image by using a Gaussian smooth filter and a down sampling operator. This is a common way of simulating LR images in MRI super-resolution [6]. In experiments, the Gaussian smooth filter is in the size of 3×3 with standard deviation of 1 and the down-sampling factor of 2. The LR image is interpolated by CGI because CGI takes an important factor, edge contrast, into interpolation and effectively avoid image artifacts with fairly low computational complexity.

The purpose of our method is to recover edge details of LR brain image. In our work, a pixel is declared to be an edge pixel if the local variance within its nearest neighbors is greater than or equal to an established threshold of 0.0003,

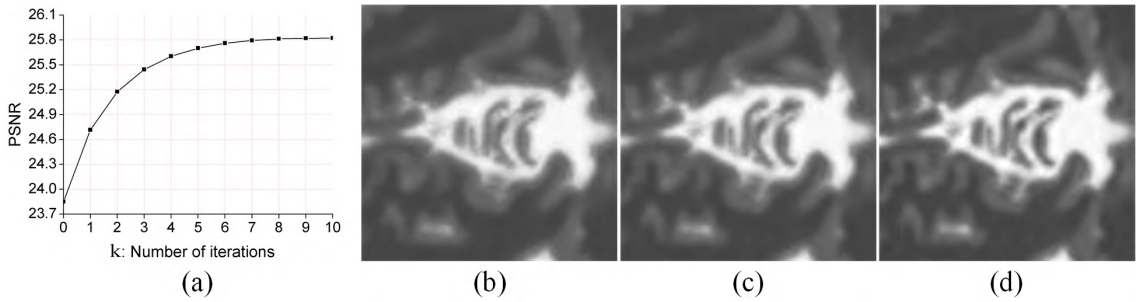

FIGURE 7. Magnified regions of reconstruction results versus the number of iterations k. (a) The PSNRs of using IBP versus the different k. The bottom row shows a zoom-up region in the reconstruction result and from left to right: (b) $k = 0$ (i.e., without IBP); (c) $k = 1$; (d) $k = 5$.

on the premise that intensities of images are all normalized between 0 and 1. The same value of the threshold is utilized in all experiments of this paper.

B. COMPARISONS WITH OTHER METHODS

Brainweb [25] (http://www.bic.mni.mcgill.ca/brainweb/) is a publicly available dataset which provides two kinds of MRI simulated image: normal (e.g., Imag_B1 and Imag_B2) and multiple sclerosis (e.g., Imag_B3 and Imag_B4). A note about multiple sclerosis lesions data is that they have been extracted from real MRI data. The data of in-plane pixel size is automatically set as 1 × 1mm. In addition, we select noise percentages of 1%. The original 2D T1w and T2w data are in the size of 181 × 217.

We also assess the performance of our algorithm on real brain MRI images which have four types:

1) IMAGING DATA SHARED BY PHILIPS COMPANY

Imag_H1 and Imag_H2 (noting: test images of TABLE 1 in the revision are numbered) are shared by Philips Company. The T1w (TR = 170 ms, TE = 3.9ms) and T2w (TR = 3000ms, TE = 80ms) images of 256 × 256 size are acquired with fast field echo sequence (FOV = 230 × 230 mm2, slice thickness = 5.0 mm).

2) IMAGING DATA FROM SIEMENS SCANNERS

Imag_P1 and Imag_P2 are acquired from a 3T Siemens Trio Tim MRI scanner using a turbo spin echo sequence (FOV = 230 × 187 mm2, slice thickness = 5.0mm) and the matrix size of original T1w (TR = 2000ms, TE = 9.7ms) and T2w (TR = 5000ms, TE = 97ms) images is 384 × 324.

3) PUBLIC NAMIC DATA

Imag_N1 and Imag_N2 are acquired from – a publicly available MRI brain dataset (http://hdl.handle.net/1926/1687), which is provided by National Alliance for Medical Image Computing (NAMIC). The dataset is acquired at a 3T GE scanner at BWH in Boston, MA, and contains 10 normal persons and 10 schizophrenic patients. The matrix size of the T1w (TR = 7.4 ms, TE = 3 ms) or T2w (TR = 2500 ms, TE = 80 ms) data is 256 × 256×176, with voxel resolution of 1 × 1×1 mm3. In this paper, two 2D brain images are acquired from extracting 3D data along the coronal plane.

4) IMAGING DATA FROM EAST CHINA NORMAL UNIVERSITY

Imag_E1 and Imag_E2 are from East China Normal University dataset (ECNU_set). The experiments were carried out on a 3 T MRI scanner (Siemens Trio Tim), with FOV of 256 × 256 mm2. The acquired dataset includes T1w (TR = 440 ms, TE = 2.46 ms) and T2w (TR = 6750 ms, TE = 90 ms) images with 3mm slice, and also T1w (TR = 250 ms, TE = 2.46 ms) and T2w (TR = 4500 ms, TE = 90 ms) images with 4 mm slice. All images are with pixel size of 256 × 256. The T1w and T2w data are acquired with gradient echo pulse sequence and turbo spin echo sequence, respectively.

these 1), 2), and 4) studies were respectively approved by Institutional Review Board of Philips Company, Shenzhen Institutes of Advanced Technology, and East China Normal University. Their proper informed consents were obtained from all volunteers prior to enrollment.

To better display edge structures in the experimental results, we provide zoom-in images (Fig. 8). Among them, reconstructions of normal and multiple sclerosis anatomical datasets are depicted in Figs. 8 (a) and (b), respectively. Results on real datasets are presented in Figs. 8 (c)-(e). From top to bottom are the result of the bicubic, CGI, ILWS, the proposed method without the IBP, the proposed method with the IBP, the ground truth image and HR reference image. Full figures are given in the appendix C.

In Fig. 8, the bicubic method (1st row) results in more blur structure details than other methods. ILWS (3rd row) achieves sharper edges compared to the bicubic, but the ringing artifacts can still be observed along the edges. Furthermore, CGI (2nd row) recovers edges better than ILWS. Obviously, the proposed algorithm without IBP (4th row) delivers more subjective results with sharp edges than CGI. In addition, details of edge structures are further clearly revealed in results of the proposed method with IBP (5th row).

TABLE 1 summarizes the PSNR and SSIM values for image interpolation. It shows that ILWS obtains higher PSNR and SSIM than classic bicubic, but CGI outperforms

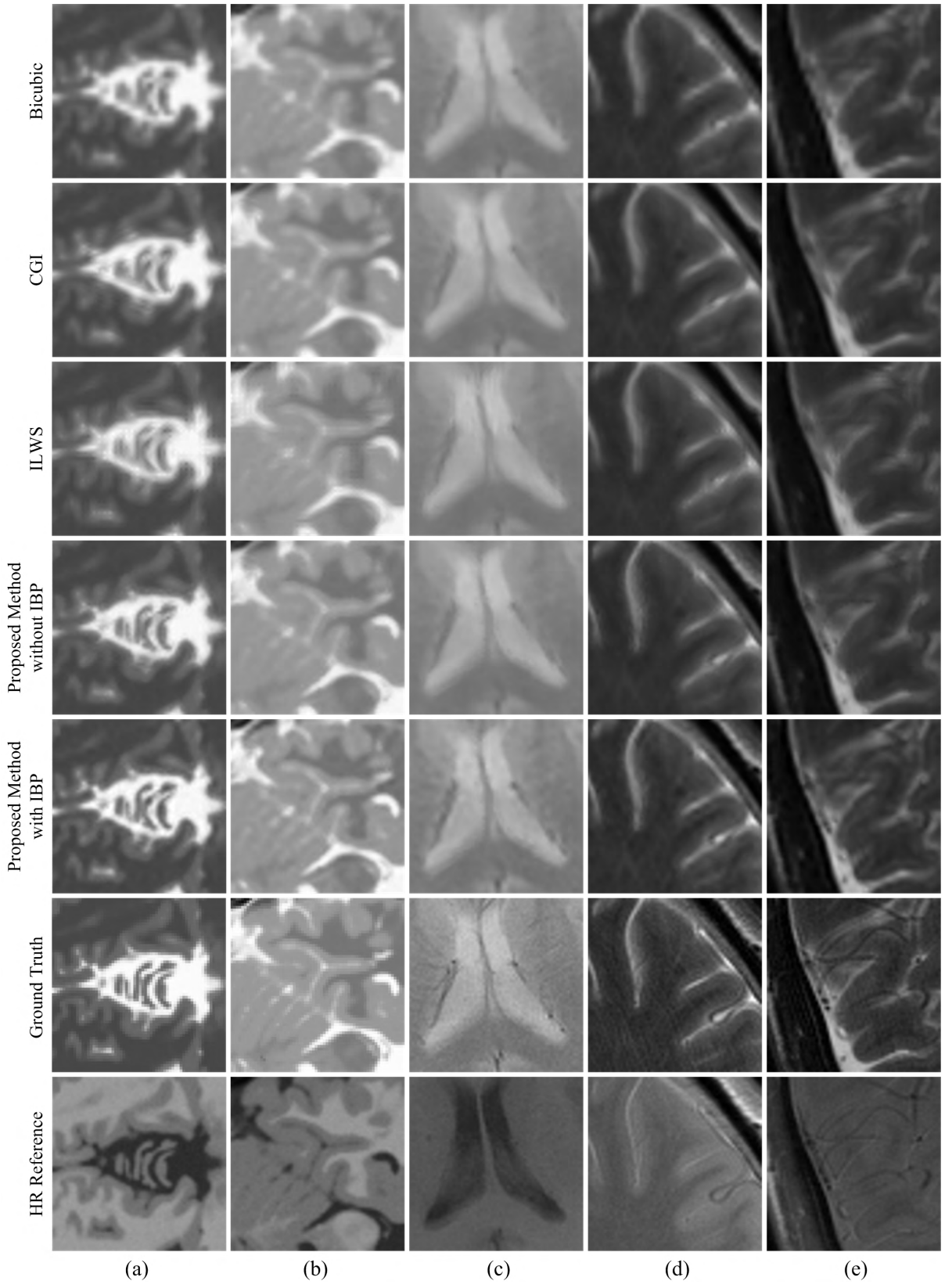

FIGURE 8. Magnified sections of reconstructed images. Among them, (a-b) are respectively results of Imag_B1 and Imag_B3 from the Brainweb dataset; (c-e) are based on the real data and are results of Imag_H1, Imag_P1 and Imag_P2. From top to bottom: Bicubic; CGI; ILWS; the proposed method without IBP; the proposed method with IBP; the ground truth image; the HR reference image.

TABLE 1. PSNR/SSIM evaluation for defferent methods.

Images		Bicubic	CGI	ILWS	Proposed Method without IBP	Proposed Method with IBP
Brainweb	Imag_B1	20.98/0.7891	23.43/0.8612	22.44/0.8424	23.85/0.8752	**25.70/0.9036**
	Imag_B2	20.95/0.7831	23.53/0.8513	22.68/0.8363	23.92/0.8641	**25.94/0.8926**
	Imag_B3	22.09/0.7934	24.62/0.8685	23.65/0.8497	25.03/0.8835	**26.84/0.9146**
	Imag_B4	21.98/0.7887	24.76/0.8525	23.88/0.8373	25.25/0.8645	**27.29/0.8906**
Real	Imag_H1	28.53/0.8682	30.71/0.8996	30.48/0.8946	31.28/0.9087	**32.27/0.9243**
	Imag_H2	28.72/0.8831	31.35/0.9126	31.06/0.9071	31.85/0.9181	**32.96/0.9320**
	Imag_P1	30.59/0.9101	32.89/0.9320	32.60/0.9274	33.98/0.9391	**35.20/0.9488**
	Imag_P2	29.38/0.8950	31.89/0.9224	31.61/0.9173	33.13/0.9309	**34.43/0.9435**
	Imag_N1	29.10/0.8960	31.45/0.9341	30.62/0.9197	32.03/0.9419	**33.62/0.9583**
	Imag_N2	29.43/0.9000	31.99/0.9378	31.12/0.9245	32.61/0.9454	**34.34/0.9606**
	Imag_E1	28.95/0.9131	31.68/0.9443	31.20/0.9381	32.61/0.9517	**34.33/0.9641**
	Imag_E2	29.51/0.9146	31.77/0.9428	31.38/0.9365	32.76/0.9514	**34.44/0.9643**

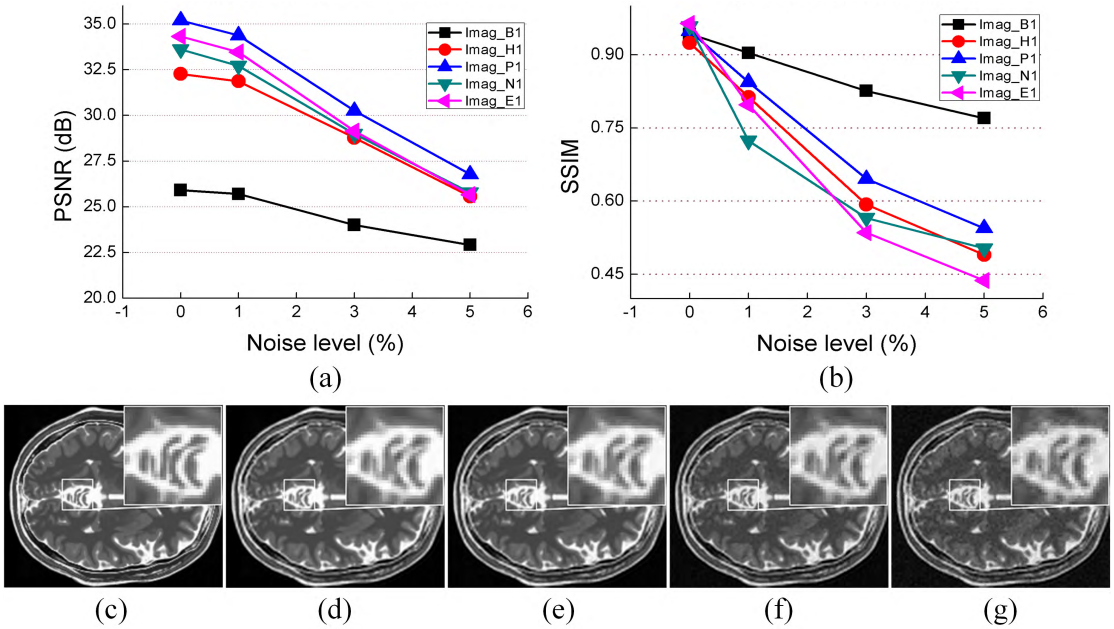

FIGURE 9. Effects of noise on the proposed method. (a) and (b) are PSNR and SSIM performance. Noting: Noise are randomly generated for 30 times and the PSNR and SSIM are averaged over the 30 super-resolution experiments. Visual results based Imag_B1with different noise level are presented in (c-g): 0%, 1%, 3% and 5% noise, respectively. Note: IBP is imbedded in the proposed method.

both Bicubic and ILWS. The proposed method, however without IBP or with IBP, outperforms the other three methods.

V. DISCUSSIONS

In this section, we first evaluate the effect of noise on the proposed method, and then extend the comparison with a state-of-the art non-local MRI upsampling techniques, and finally report the the computational time of different methods.

A. EFFECTS OF NOISE

The noise at common levels (0%, 1%, 3% and 5% of the maximum intensity) [31], [32] are added into the T2-weighted ground truth image. To simulate the Rician noise in real data (Imag_H1, Imag_P1, Imag_N1, and Imag_E1) [31], [32], the zero mean Gaussian noise are added to real and imaginary parts of ground truth images, respectively.

Results on different level noise (Figs. 9 (a) and (b)) imply that increasing the noise level will reduce the PSNR and SSIM. These two criteria are seriously reduced when the

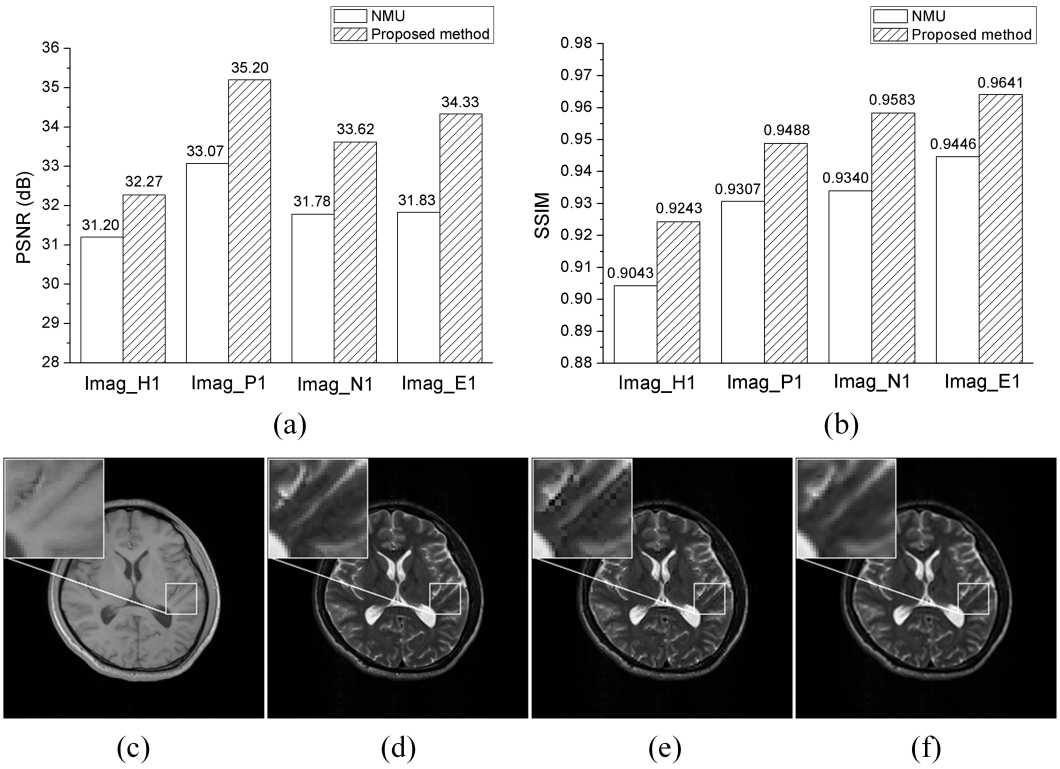

FIGURE 10. Comparison with NMU. (a) and (b) are PSNR and SSIM performance, respectively. Visual results based Imag_E1 are presented in (c-f): HR reference image, ground truth image, NMU, and proposed method. Note: CGI-based pre-interpolation and IBP are imbedded in the proposed method.

TABLE 2. Reconstruction performance (PSNR/SSIM) on degraded images with average filtering.

Images	CGI	NMU	Proposed Method	
			(CGI pre-interpolation)	(NMU pre-interpolation)
Imag_H1	28.97/0.8828	32.28/0.9232	29.61/0.8939	**32.43/0.9265**
Imag_P1	30.95/0.9168	34.16/0.9435	31.83/0.9255	**34.99/0.9477**
Imag_N1	29.25/0.9060	33.21/0.9557	29.83/0.9164	**33.30/0.9565**
Imag_E1	29.57/0.9270	33.66/0.9629	30.45/0.9356	**33.98/0.9640**

Note: The size of average filtering is 2×2, IBP is not applied in the proposed method

noise level is equal or greater than 3%, indicating obvious degraded images in Figs. 9 (f) and (g).

B. COMPARISON WITH NON-LOCAL UPSAMPLING

we add the comparison with the method "Non-local MRI upsampling" [10], which is referred as NMU here. Since NMU is a super-resolution algorithm for degraded 3D MRI images with average filtering, we rewrite it into a 2D algorithm with Gaussian filtering for facilitating the comparison.

Results in Figs. 10 (a) and (b) show that the NMU obtains good PSNR and SSIM values and proposed method achieves better evaluation criteria than the NMU. To further verify the performance, super-resolved images are reported in Figs. 10 (e) and (f), indicating that the proposed method provides more consistent image structures to the ground-truth image shown in (Fig. 10 (d)).

It is worth noting that, NMU performs very well on the degraded images with average filtering, which is the problem originally discussed in [10], as shown in TABLE 2. With the NMU is as the pre-interpolation, the proposed method can still improve the super-resolved images.

C. COMPUTATION TIME

The computation time of different methods are shown in TABLE 3. Traditional methods consume no more than 2 seconds while the proposed method requires 35 seconds. Thus, the new method is relatively time consuming.

TABLE 3. Computation time for defferent methods (units: seconds).

	Images		Bicubic	CGI	ILWS	Proposed Method without IBP	Proposed Method with IBP
Brainweb	Imag_B1	256×256	**0.091**	0.066	1.605	36.554	36.581
	Imag_B2	256×256	**0.002**	0.063	1.451	35.148	35.160
	Imag_B3	256×256	**0.002**	0.058	1.602	41.690	41.702
	Imag_B4	256×256	**0.002**	0.059	1.496	33.780	33.791
Real	Imag_H1	256×256	**0.002**	0.100	2.451	16.898	16.912
	Imag_H2	256×256	**0.002**	0.094	2.383	16.596	16.613
	Imag_P1	384×324	**0.002**	0.184	4.928	93.021	93.039
	Imag_P2	384×324	**0.003**	0.164	4.952	85.791	85.813
	Imag_N1	256×176	**0.002**	0.066	1.564	22.583	22.594
	Imag_N2	256×176	**0.002**	0.066	1.539	18.663	18.675
	Imag_E1	256×256	**0.002**	0.094	2.407	19.049	19.064
	Imag_E2	256×256	**0.002**	0.095	2.374	19.350	19.363

VI. CONCLUSION

We proposed a new super-resolution method for MRI multi-contrast images by using gradient information of the high-resolution reference image that has another contrast. The connection of gradient value between different MRI contrast images is studied and an associated model is established to estimate values of edge pixels inside the pre-interpolated image. Experimental results demonstrate that the proposed algorithm is effective for both synthetic and real MRI images. The IBP filter is suggested to be applied after our algorithm to further improve the quality of super-resolved MRI images.

In this work, the proposed method is mainly developed for 2D MRI images. Extension and application of this algorithm on 3D data will be an interesting future work. In addition, how to retrieve structural distinctions hidden in multi-contrast MRI images more accurately still need further investigation. Last, this modeling may benefit improving reconstruction of fast imaging in MRI [22], [33]–[38] and reconstruction of multi-contrast MRI images in fast sampling [39]–[41].

ACKNOWLEDGMENTS

The authors sincerely thank Dr. Kai-Kuang Ma for sharing CGI code, Dr. Kaihua Zhang for providing the data in Fig.C5 and Kourosh Jafari-Khouzani for valuable suggestions. They also appreciate reviewers for their constructive comments.

REFERENCES

[1] H. Greenspan, "Super-resolution in medical imaging," *Comput. J.*, vol. 52, no. 1, pp. 43–62, 2009.

[2] S. Yu, R. Zhang, S. Wu, J. Hu, and Y. Xie, "An edge-directed interpolation method for fetal spine MR images," *BioMed. Eng. Online*, vol. 12, p. 102, Oct. 2013.

[3] Y.-H. Wang, J. Qiao, J. Li, P. Fu, S.-C. Chu, and J. F. Roddick, "Sparse representation-based MRI super-resolution reconstruction," *Measurement*, vol. 47, pp. 946–953, Jan. 2014.

[4] D. Zhang, J. He, Y. Zhao, and M. Du, "MR image super-resolution reconstruction using sparse representation, nonlocal similarity and sparse derivative prior," *Comput. Boil. Med.*, vol. 58, pp. 130–145, Mar. 2015.

[5] X. Lu, Z. Huang, and Y. Yuan, "MR image super-resolution via manifold regularized sparse learning," *Neurocomputing*, vol. 162, pp. 96–104, Aug. 2015.

[6] A. Rueda, N. Malpica, and E. Romero, "Single-image super-resolution of brain MR images using overcomplete dictionaries," *Med. Image Anal.*, vol. 17, no. 1, pp. 113–132, 2013.

[7] K. Jafari-Khouzani, "MRI upsampling using feature-based nonlocal means approach," *IEEE Trans. Med. Imag.*, vol. 33, no. 10, pp. 1969–1985, Oct. 2014.

[8] S. Tourbier, X. Bresson, P. Hagmann, J.-P. Thiran, R. Meuli, and M. B. Cuadra, "An efficient total variation algorithm for super-resolution in fetal brain MRI with adaptive regularization," *NeuroImage*, vol. 118, pp. 584–597, Sep. 2015.

[9] F. Shi, J. Cheng, L. Wang, P.-T. Yap, and D. Shen, "LRTV: MR image super-resolution with low-rank and total variation regularizations," *IEEE Trans. Med. Imag.*, vol. 34, no. 12, pp. 2459–2466, Dec. 2015.

[10] J. V. Manjón, P. Coupé, A. Buades, V. Fonov, D. L. Collins, and M. Robles, "Non-local MRI upsampling," *Med. Image Anal.*, vol. 14, no. 6, pp. 784–792, 2010.

[11] Y. Jia, A. Gholipour, Z. He, and S. K. Warfield, "A new sparse representation framework for reconstruction of an isotropic high spatial resolution MR volume from orthogonal anisotropic resolution scans," *IEEE Trans. Med. Imag.*, vol. 36, no. 5, pp. 1182–1193, May 2017.

[12] Z. Mai, J. Rajan, M. Verhoye, and J. Sijbers, "Robust edge-directed interpolation of magnetic resonance images," *Phys. Med. Biol.*, vol. 56, no. 22, pp. 7287–7303, 2011.

[13] F. Rousseau, "Brain hallucination," in *Proc. Comput. Vis. ECCV*, vol. 8, 2008, pp. 497–508.

[14] F. Rousseau and The Alzheimer's Disease Neuroimaging Initiative, "A non-local approach for image super-resolution using intermodality priors," *Med. Image Anal.*, vol. 14, no. 4, pp. 594–605, Aug. 2010.

[15] C. Hu, X. Qu, D. Guo, L. Bao, and Z. Chen, "Wavelet-based edge correlation incorporated iterative reconstruction for undersampled MRI," *Magn. Reson. Imag.*, vol. 29, no. 7, pp. 907–915, Sep. 2011.

[16] Z. Wei and K.-K. Ma, "Contrast-guided image interpolation," *IEEE Trans. Image Process.*, vol. 22, no. 11, pp. 4271–4285, Nov. 2013.

[17] J. V. Manjón, P. Coupé, A. Buades, D. L. Collins, and M. Robles, "MRI superresolution using self-similarity and image priors," *Int. J. Biomed. Imag.*, vol. 2010, Oct. 2010, Art. no. 425891.

[18] H. Zheng *et al.*, "Multi-contrast brain magnetic resonance image super-resolution using the local weight similarity," *BMC Med. Imag.*, vol. 17, no. 1, p. 6, 2017, doi: 10.1186/s12880-016-0176-2.

[19] C. Shi, F. Liu, L. Li, L. Jiao, Y. Duan, and S. Wang, "Learning interpolation via regional map for pan-sharpening," *IEEE Trans. Geosci. Remote Sens.*, vol. 53, no. 6, pp. 3417–3431, Jun. 2015.
[20] A. Wong, A. Mishra, P. Fieguth, and D. A. Clausi, "Sparse reconstruction of breast MRI using homotopic L_0 minimization in a regional sparsified domain," *IEEE Trans. Biomed. Eng.*, vol. 60, no. 3, pp. 743–752, Mar. 2013.
[21] M. A. Brown and R. C. Semelka, *MRI Basic Principles and Applications*. Hoboken, NJ, USA: Wiley, 2003.
[22] X. Qu, Y. Hou, F. Lam, D. Guo, J. Zhong, and Z. Chen, "Magnetic resonance image reconstruction from undersampled measurements using a patch-based nonlocal operator," *Med. Image Anal.*, vol. 18, pp. 843–856, Aug. 2014.
[23] W. Yang *et al.*, "Improving low-dose CT image using residual convolutional network," *IEEE Access*, vol. 5, pp. 24698–24705, 2017.
[24] X. Fan, Q. Lian, and B. Shi, "Compressed sensing MRI with phase noise disturbance based on adaptive tight frame and total variation," *IEEE Access*, vol. 5, pp. 19311–19321, 2017.
[25] C. A. Cocosco, V. Kollokian, R. K.-S. Kwan, and A. C. Evans, "BrainWeb: Online interface to a 3D MRI simulated brain database," *Neuroimage*, vol. 5, no. 4, p. 425, 1997.
[26] X. Qu *et al.*, "Undersampled MRI reconstruction with patch-based directional wavelets," *Magn. Reson. Imag.*, vol. 30, no. 7, pp. 964–977, Sep. 2012.
[27] Z. Zhan, J.-F. Cai, D. Guo, Y. Liu, Z. Chen, and X. Qu, "Fast multiclass dictionaries learning with geometrical directions in MRI reconstruction," *IEEE Trans. Biomed. Eng.*, vol. 63, no. 9, pp. 1850–1861, Sep. 2016.
[28] H. Greenspan, G. Oz, N. Kiryati, and S. Peled, "MRI inter-slice reconstruction using super-resolution," *Magn. Reson. Imag.*, vol. 20, no. 5, pp. 437–446, Jun. 2002.
[29] M. Irani and S. Peleg, "Motion analysis for image enhancement: Resolution, occlusion, and transparency," *J. Vis. Commun. Image Represent.*, vol. 4, no. 4, pp. 324–335, Dec. 1993.
[30] Z. Wang, A. C. Bovik, H. R. Sheikh, and E. P. Simoncelli, "Image quality assessment: From error visibility to structural similarity," *IEEE Trans. Image Process.*, vol. 13, no. 4, pp. 600–612, Apr. 2004.
[31] J. V. Manjón, J. Carbonell-Caballero, J. J. Lull, G. García-Martí, L. Martí-Bonmatí, and M. Robles, "MRI denoising using non-local means," *Med. Image Anal.*, vol. 12, no. 4, pp. 514–523, 2008.
[32] H. Gudbjartsson and S. Patz, "The Rician distribution of noisy MRI data," *Mag. Reson. Med.*, vol. 34, no. 6, pp. 910–914, 1995.
[33] Y. Liu, Z. Zhan, J.-F. Cai, D. Guo, Z. Chen, and X. Qu, "Projected iterative soft-thresholding algorithm for tight frames in compressed sensing magnetic resonance imaging," *IEEE Trans. Med. Imag.*, vol. 35, no. 9, pp. 2130–2140, Sep. 2016.
[34] Y. Zhang, Z. Dong, P. Phillips, S. Wang, G. Ji, and J. Yang, "Exponential wavelet iterative shrinkage thresholding algorithm for compressed sensing magnetic resonance imaging," *Inf. Sci.*, vol. 332, pp. 115–132, Nov. 2015.
[35] Z. Chen *et al.*, "Joint reconstruction of multi-contrast images and multi-channel coil sensitivities," *Appl. Magn. Reson.*, vol. 48, no. 9, pp. 955–969, 2017.
[36] Y. Yang *et al.*, "Pseudo-polar Fourier transform-based compressed sensing MRI," *IEEE Trans. Biomed. Eng.*, vol. 64, no. 4, pp. 816–825, Apr. 2017.
[37] M. Lustig, D. Donoho, and J. M. Pauly, "Sparse MRI: The application of compressed sensing for rapid MR imaging," *Magn. Reson. Med.*, vol. 58, no. 6, pp. 1182–1195, 2007.
[38] Y. Liu, C. Ma, B. Clifford, F. Lam, C. L. Johnson, and Z.-P. Liang, "Improved low-rank filtering of magnetic resonance spectroscopic imaging data corrupted by noise and B_0 field inhomogeneity," *IEEE Trans. Biomed. Eng.*, vol. 63, no. 4, pp. 841–849, Apr. 2016.
[39] Z. Lai *et al.*, "Image reconstruction of compressed sensing MRI using graph-based redundant wavelet transform," *Med. Image Anal.*, vol. 27, pp. 93–104, Jan. 2016.
[40] Z. Lai *et al.*, "Sparse MRI reconstruction using multi-contrast image guided graph representation," *Magn. Reson. Imag.*, vol. 43, pp. 95–104, Nov. 2017.
[41] X. Qu, W. Zhang, D. Guo, C. Cai, S. Cai, and Z. Chen, "Iterative thresholding compressed sensing MRI based on contourlet transform," *Inverse Problems Sci. Eng.*, vol. 18, no. 6, pp. 737–758, 2010.

HONG ZHENG received the B.S. degree from the Guilin University of Electronic Technology, Guilin, China, in 2007. She is currently pursuing the Ph.D. degree with the Department of Electronic Science, College of Physical Science and Technology, Xiamen University, Xiamen, China. She is also a Lecturer with the Key Laboratory of Intelligent Processing of Image and Graphics, School of Computer Science and Information Security, Guilin University of Electronic Technology. Her research interests include medical image reconstruction and signal and image processing. She received the Student Travel Award of ISMRA in 2015.

KUN ZENG received the B.Eng., M.Sc., and Ph.D. degrees from the Department of Computer Science, Xiamen University, Xiamen, China, in 2005, 2008, and 2012, respectively. He currently holds a post-doctoral position with the Department of Electronic Science, Xiamen University. His current research interests include MRI reconstruction, image processing, and machine learning.

DI GUO received the B.S. and Ph.D. degrees in communication engineering from Xiamen University, China, in 2005 and 2012, respectively. From 2009 to 2011, she was a Visiting Scientist with the Department of Electrical Engineering, University of Washington, Seattle, USA. She is currently an Associate Professor with the Department of Computer Science and Technology, Xiamen University of Technology, China. Her research interests include signal and image processing, and their applications in biomedical engineering, wireless sensor networks, and Internet of Things. She received the IBM Distinguished Student Award in 2012.

JIAXI YING received the B.S. degree from the School of Science, Nanjing University of Science and Technology, in 2012, and the M.S. degree from the Department of Electronic Science, Xiamen University, in 2017. Since 2017, he has been a Research Assistant with the Department of Mathematics, The Hong Kong University of Science and Technology, Hong Kong. His research interests include optimization, statistical signal processing, information theory, harmonic analysis, and their applications to machine learning, medical imaging, and inverse problems.

YU YANG was born in Zhangzhou, Fujian, China, in 1982. She received the B.S. degree in acoustics from Nanjing University, China, in 2004, and the Ph.D. degree in electrical engineering from Tsinghua University, Beijing, China, in 2009. Since 2015, she has been an Assistant Professor with the Electronic Science Department, Xiamen University, Xiamen, China. Her research interests include signal processing, evolutionary algorithms, magnetic resonance, and electromagnetic transients.

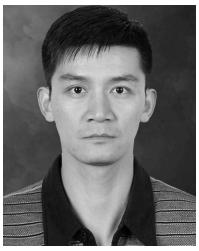

XI PENG received the B.E. and M.S. degrees in measurement, control and instruments and the Ph.D. degree in electrical engineering from Wuhan University, Wuhan, China, in 2006, 2008, and 2012, respectively. He was a Visiting Scholar with the Beckman Institute, University of Illinois at Urbana–Champaign, Urbana, IL, USA. He is currently an Associate Professor with the Paul C. Lauterbur Research Center for Biomedical Imaging, Institute of Biomedical and Health Engineering, Shenzhen Institutes of Advanced Technology, Chinese Academy of Sciences, Shenzhen, China. His current research interests include image reconstruction, parameter estimation, and signal processing for biomedical applications.

FENG HUANG received the Ph.D. degree from the Department of Mathematics, University of Florida, in 2004. From 2004 to 2016, he served as a Senior Research Scientist, a Principal Scientist, and the Director of the MR method at Philips Healthcare. He is currently the Chief Scientist and the Director of the MR Clinical Excellence Team and the AI Center, Neusoft Medical System. His research interests include techniques and applications of medical imaging, medical image processing, and artificial intelligence.

ZHONG CHEN received the Ph.D. degree from Xiamen University, China, in 1993. In 1995, he joined Xiamen University as an Associate Professor and was appointed as the Director of the Magnetic Resonance Center. From 1998 to 2000, he was a Visiting Associate Professor with the University of Rochester, USA, where he has been a Full Professor with the Department of Physics/Electronic Science since 2000. His research interests are centered on nuclear magnetic resonance techniques and applications.

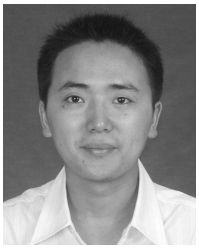

XIAOBO QU received the B.S. and Ph.D. degrees in communication engineering from Xiamen University, China, in 2006 and 2011, respectively. From 2009 to 2011, he was a Visiting Scholar with the Department of Electrical and Computer Engineering, University of Illinois at Urbana–Champaign. Since 2012, he has been a Faculty Member with Xiamen University, where he is currently an Associate Professor with the Department of Electronic Science, the Research Center of Magnetic Resonance and Medical Imaging, and the Research Center for Molecular Imaging and Translational Medicine. In 2014, he was the Visiting Scientist with the Swedish NMR Centre, University of Gothenburg, Sweden. His research interests include magnetic resonance imaging and spectroscopy, signal and image representations, computational imaging, machine learning, and artificial intelligence. He has been a member of ISMRM, IEEE EMBS, and SPS. He received the E. K. Zavoisky Stipend of ISMRM Scientific Meeting in 2014, 2016, and 2018, the Swedish Wenner-Gren Fellowship in 2014, the Distinguished Young Scholar Award from the Natural Science Foundation of Fujian Province of China in 2017, and the Faculty Research Award in 2014 and the He Yici Chair Professor Award in 2018 from Xiamen University, respectively. He is an Associate Editor of the IEEE TRANSACTIONS ON COMPUTATIONAL IMAGING and a Section Editor of *BMC Medical Imaging*. He is on the Editorial Board of *Quantitative Imaging in Medicine and Surgery*.